Available online at www.sciencedirect.com
ScienceDirect
Journal of Hydrodynamics
2014,26(5):669-680
DOI: 10.1016/S1001-6058(14)60075-5
www.sciencedirect.com/science/journal/l0016058

Entropy generation in bypass transitional boundary layer flows*

GEORGE Joseph, OWEN Landon D., XING Tao
Department of Mechanical Engineering, College of Engineering, University of Idaho, Moscow, Idaho 83843, USA, E-mail: geor6350@vandals.uidaho.edu
MCELIGOT Donald M.
University of Idaho, Idaho Falls, Idaho 83402, USA
CREPEAU John C.
Department of Mechanical Engineering, College of Engineering, University of Idaho, Moscow, Idaho 83843, USA
BUDWIG Ralph S.
University of Idaho, Boise, Idaho 83702, USA
NOLAN Kevin P.
Imperial College London, London SW7-28Z, UK

(Received June 22, 2014, Revised September 25, 2014)

Abstract: The primary objective of this study is to evaluate the accuracy of using computational fluid dynamics (CFD) turbulence models to predict entropy generation rates in bypass transitional boundary layers flows under zero and adverse pressure gradients. Entropy generation rates in such flows are evaluated employing the commercial CFD software, ANSYS FLUENT. Various turbulence and transitional models are assessed by comparing their results with the direct numerical simulation (DNS) data and two recent CFD studies. A solution verification study is conducted on three systematically refined meshes. The factor of safety method is used to estimate the numerical error and grid uncertainties. Monotonic convergence is achieved for all simulations. The Reynolds number based on momentum thickness, Re_θ, skin-friction coefficient, C_f, approximate entropy generation rates, S''', dissipation coefficient, C_d, and the intermittency, γ, are calculated for bypass transition simulations. All Reynolds averaged Navier-Stokes (RANS) turbulence and transitional models show improvement over previous CFD results in predicting onset of transition. The transition SST k-ω 4 equation model shows closest agreement with DNS data for all flow conditions in this study due to a much finer grid and more accurate inlet boundary conditions. The other RANS models predict an early onset of transition and higher boundary layer entropy generation rates than the DNS shows.

Key words: entropy generation, bypass transition, Reynolds averaged Navier-Stokes (RANS), transitional boundary layer, turbulence models

Introduction

Entropy is the property that serves as a measure of disorder within a system. Entropy generation therefore causes irreversible loss of energy in fluid flows. Determining and minimizing these losses improves the efficiency of a system[1]. Systems that benefit from the minimization of entropy generation include: cooling systems for electronic devices and nuclear reactors, thermal heat exchangers, and more. Four different mechanisms contribute to entropy generation: Mean and fluctuating heat flux and Mean and fluctuating viscous effects. Steady, unheated, laminar flow has zero fluctuations so the entropy generation occurs only from the viscous losses associated with mean velocity gradients. Bypass transition occurs when freestream vortical disturbances induce transition to turbulence in a boundary layer without the intervention of viscous Tollmien-Schlichting waves[2]. Viscous losses associated with the mean and fluctuating velocity gradients cause entropy generation in bypass transitional

* **Biography:** GEORGE Joseph (1986-), Male, Master Candidate
Corresponding author: XING Tao, E-mail: xing@uidaho.edu

boundary layer flows. Many different methods exist to predict entropy generation in fluid systems.

Direct numerical simulation (DNS) is a proven tool in elucidating flow physics. DNS completely resolves all of the laminar and turbulent length scales and thus can be used as a numerical benchmark to evaluate the accuracy of simulations using various turbulence models. McEligot et al.[3] analyzed DNS results from two different studies conducted by Spalart[4,5] of turbulent boundary layer flows with zero and favorable pressure gradients with Re_θ ranging from 300 to 1 410. The study found that approximately two-thirds of the entropy generation occurs in the viscous layer of a turbulent boundary layer (defined as $y^+ \approx 30$). The study demonstrated that entropy dissipation is nearly universal within the viscous layer of turbulent boundary layer flows with zero and favorable pressure gradients. The study showed that the methodology developed by Rotta[6] for approximating S''' is inaccurate for the given flow characteristics. McEligot et al.[7] similarly analyzed results from a DNS[8] of turbulent channel flow with zero and favorable pressure gradients. McEligot compared two methods for determining entropy generation. The first method evaluated the fluctuating gradients forming the dissipation term in the turbulent enthalpy equation and the second method evaluated an approximate analogy to laminar flow employing assumed boundary layer (and other) approximations[9]. Both methods predict similar S'' values. The second method under-predicted entropy generation in the "linear" layer and over-predicted entropy generation in the rest of the viscous layer.

Another study by McEligot et al.[10] compared the entropy generation predicted from a DNS of turbulent boundary layer flow to the entropy generation predicted from a DNS of channel flow[8,11]. The study demonstrated that the pointwise entropy generation at the boundary of the viscous layer is relatively insensitive for both boundary layer and channel flows with large favorable pressure gradients. The integral over the area of the viscous layer decreased moderately only for boundary layer flows. Walsh and McEligot[12] improved an existing correlation for the dissipation coefficient, C_d, using data from multiple DNS studies of low Re_θ turbulent boundary layer and channel flows with zero and favorable pressure gradients[4,8,13,14]. Walsh et al.[1] analyzed a DNS of bypass transitional boundary layer flows for Re_θ ranging from 115 to 520[15,16]. The study demonstrated that the term for turbulent convection in the turbulent kinetic energy (TKE) balance is significant within the transition region. This is as a consequence of more turbulent energy being produced than dissipated. The study showed that a popular approximation method over-estimates the dissipation coefficient by as much as 17%. The study demonstrated that the approach developed by Rotta[6] is more accurate for transitional boundary layers.

A DNS of bypass transition was performed by Zaki and Durbin[2]. This simulation showed that high-frequency, freestream fluctuations are kept from entering the boundary layer due to "shear sheltering." The study evaluated the coupling coefficient between continuous spectrum Orr-Somerfield and squire modes. The study demonstrated that a strongly and weakly coupled high-frequency mode is required to simulate the transition process completely. The bypass transition simulations here are compared to a DNS by Nolan and Zaki[17]. The DNS study used a computational domain size of $(L_x, L_y, L_z)/\delta_0 = (900, 40, 30)$ with a grid resolution of $(n_x, n_y, n_z) = (3072, 192, 192)$. The spatial resolution was $(\Delta x^+, \Delta y^+, \Delta z^+) = (11.7, \geq 0.40, 6)$. The inlet mean velocity Blasius profile was created based on $Re_{\delta 0} = 800$ with a turbulent intensity of 3%. The study tracked down turbulent spots resulting from high-amplitude streaks upstream. The study found that the volumetric growth rate of turbulent spots is insensitive to the pressure gradient.

Two recent CFD studies by Ghasemi et al.[18,19] evaluated the accuracy of different turbulence and transitional models for predicting boundary layer behavior and entropy generation in bypass transition, including the k-ε model, the SST k-ω model, the k-ω 4 equation model, the k-kl-ω 3 equation model, and the Reynolds stress model (RSM). The mesh used in the study had 149 089 grid points on a two-dimensional, zero pressure gradient domain equal to $L_x/\delta_0 = 900$ in the streamwise direction and an adverse pressure gradient domain equal to $L_x/\delta_0 = 600$ in the streamwise direction. The inlet boundary condition specified a turbulent intensity of 3% with a turbulent length scale equal to the boundary layer thickness at the inlet. These studies showed that the RANS models predict the onset of transition much earlier than the corresponding DNS[17]. The RANS models over-predicted the integral entropy generation rate and the skin friction coefficient in the transition region.

The objective of the current study is to evaluate the accuracy of various turbulence models to predict entropy generation and location of transition within a bypass transitional boundary layer. The commercial CFD software ANSYS FLUENT is employed for simulations. The flow modeled with RANS turbulence model is steady, incompressible, two-dimensional bypass transitional boundary layer flow. The RANS models employed in the study are the k-ε model, k-ω SST model, RSM model and transitional 4 equation SST k-ω model. Quantitative solution verification is conducted using three systematically refined structu-

red grids, with the finest grid containing about 10^{-6} grid points. The flow characteristics are compared to the DNS results from Nolan and Zaki[17] and two recent CFD studies by Ghasemi et al.[18,19].

1. Computational methods

1.1 *Turbulence models and numerical methods*

The non-linear Reynolds stress term is closed in the RANS models with the Boussinesq eddy viscosity hypothesis. The displacement thickness δ^*, momentum thickness θ, corresponding Reynolds number Re_θ and the Reynolds stresses are calculated as,

$$\delta^* = \int_0^\infty \left(1-\frac{u}{U_{fs}}\right)\mathrm{d}y, \quad \theta = \int_0^\infty \frac{u}{U_{fs}}\left(1-\frac{u}{U_{fs}}\right)\mathrm{d}y,$$

$$Re_\theta = \frac{\theta U_{fs}\{x\}}{\nu} \tag{1}$$

$$\overline{u_i' u_j'} = \frac{2}{3}k\delta_{ij} - \nu_t\left(\frac{\partial \overline{u}_i}{\partial x_j} + \frac{\partial \overline{u}_j}{\partial x_i}\right) \tag{2}$$

where the variable u_i is the velocity along the x, y or z axis and u_j is the velocity along an axis different from the direction of u_i. This similarly applies to x_i as the location along a given axis x, y or z. The variable δ_{ij} in the equation is the Kronecker delta and not the boundary layer thickness. The turbulent kinetic energy, k, is defined as,

$$k = \frac{\overline{u'^2} + \overline{v'^2} + \overline{w'^2}}{2} \tag{3}$$

The transport equations for the different models can be summarized as,

$$\frac{\partial}{\partial t}(\rho k) + \frac{\partial}{\partial x_i}(\rho k u_i) = \frac{\partial}{\partial x_j}\left[\left(\mu + \frac{\mu_t}{\sigma_k}\right)\frac{\partial k}{\partial x_j}\right] + G_k - Y_k \tag{4}$$

$$\frac{\partial}{\partial t}(\rho[DV]) + \frac{\partial}{\partial x_i}(\rho[DV]u_i) = \frac{\partial}{\partial x_j}\left[\left(\mu + \frac{\mu_t}{\sigma_D}\right)\frac{\partial[DV]}{\partial x_j}\right] + G_D - Y_D + D_D \tag{5}$$

where $[DV]$ is the corresponding turbulence dissipation variable for the model. The formulations for the k-ε model are described in the ANSYS FLUENT Theory Guide[20]. The transport equations for the k-ε model require the following,

$$[DV] = \varepsilon, \quad G_k = -\rho\overline{u_i' u_j'}\frac{\partial u_j}{\partial x_i}, \quad Y_k = \rho\varepsilon,$$

$$G_D = 1.44\frac{\varepsilon}{k}G_k, \quad Y_D = 1.92\rho\frac{\varepsilon^2}{k}, \quad D_D = 0,$$

$$\sigma_k = 1.0, \quad \sigma_D = 1.3 \tag{6}$$

where the turbulent viscosity is calculated as,

$$\mu_t = 0.9\rho\frac{k^2}{\varepsilon} \tag{7}$$

The transport equations for the SST k-ω model are,

$$[DV] = \omega, \quad G_k = \min\left(-\rho\overline{u_i' u_j'}\frac{\partial u_j}{\partial x_i}, 10Y_k\right),$$

$$Y_k = 0.09\rho k\omega, \quad G_D = \frac{\alpha}{\nu_t}G_k, \quad Y_D = \rho\beta\omega^2,$$

$$\sigma_k = \frac{1}{\frac{F_1}{1.176} + \frac{1-F_1}{1.0}}, \quad \sigma_D = \frac{1}{\frac{F_1}{2.0} + \frac{1-F_1}{1.168}} \tag{8}$$

The turbulent viscosity is calculated as,

$$\mu_t = \frac{\rho k}{\omega}\frac{1}{\max\left(1, \frac{S_T F_2}{0.31\omega}\right)} \tag{9}$$

In these equations, not all the variables are constants as is the case for the k-ε model. The transition SST model couples two additional transport equations with the SST k-ω transport equations. The first additional transport equation is for the intermittency, γ, defined as,

$$\frac{\partial}{\partial t}(\rho\gamma) + \frac{\partial}{\partial x_j}(\rho u_j\gamma) = \frac{\partial}{\partial x_j}\left[\left(\mu + \frac{\mu_t}{\sigma_\gamma}\right)\frac{\partial\gamma}{\partial x_j}\right] + P_{\gamma 1} - E_{\gamma 1} + P_{\gamma 2} - E_{\gamma 2} \tag{10}$$

The onset of transition is controlled by,

$$Re_V = \frac{\rho y^2 S_T}{\mu}, \quad R_T = \frac{\rho_k}{\mu\omega} \tag{11}$$

where S_T is the strain rate magnitude given as,

$$S_T = \sqrt{2S_{ij}S_{ij}}, \quad S_{ij} = \frac{1}{2}\left(\frac{\partial u_i}{\partial x_j} + \frac{\partial u_j}{\partial x_i}\right) \tag{12}$$

The second additional transport equation for the transition momentum thickness Reynolds number, $Re_{\theta t}$ is,

$$\frac{\partial}{\partial t}(\rho Re_{\theta t}) + \frac{\partial}{\partial x_j}(\rho u_j Re_{\theta t}) = \frac{\partial}{\partial x_j}\left[2(\mu+\mu_t)\frac{\partial Re_{\theta t}}{\partial x_j}\right] + P_{\theta t} \tag{13}$$

where $Re_{\theta p}$ is a proprietary empirical correlation for the transition onset and $F_{\theta t}$ is a function based on the boundary layer correlations. The transport equation for the RSM is,

$$\frac{\partial}{\partial t}(\rho\overline{u_i'u_j'}) + \frac{\partial}{\partial x_k}(\rho u_k\overline{u_i'u_j'}) = -\frac{\partial}{\partial x_k}[\rho\overline{u_i'u_j'u_k'} + \overline{p(\delta_{kj}u_i' + \delta_{ik}u_j')}] + \frac{\partial}{\partial x_k}\left[\mu\frac{\partial}{\partial x_k}(\overline{u_i'u_j'})\right] - \rho\left(\overline{u_i'u_k'}\frac{\partial u_j}{\partial x_k} + \overline{u_j'u_k'}\frac{\partial u_i}{\partial x_k}\right) + \overline{p\left(\frac{\partial u_i'}{\partial x_j} + \frac{\partial u_j'}{\partial x_i}\right)} - 2\mu\overline{\frac{\partial u_i'}{\partial x_k}\frac{\partial u_j'}{\partial x_k}} - 2\rho\Omega_k(\overline{u_j'u_m'}\varepsilon_{ikm} + \overline{u_i'u_m'}\varepsilon_{jkm}) \tag{14}$$

where ε_{ikm} and ε_{jkm} are permutation symbols. More information on the models is available within the ANSYS FLUENT Theory Guide[20].

1.2 *High performance computing*

A third-order MUSCL scheme is applied for the momentum and turbulence solvers with the pressure-velocity coupled scheme. A convergence tolerance of 10^{-10} is set for all simulations to ensure the iterative errors are much smaller than the grid errors such that the former can be neglected. Simulations are conducted using several local workstations and on University of Idaho's HPC computing resource, Big-STEM, using 8-12 core CPU's. Results are post-processed using Scilab-5.4.1 and Tecplot 360 2013.

1.3 *Iterative and statistical convergence*

Statistical convergence of the running mean on the time history of the resistance establishes statistically stationary unsteady solutions[21]. Statistical convergence for the unsteady simulation is determined using the drag coefficient, C_D, defined as,

$$C_D = \int_{x_1}^{x_2} C_f \, \mathrm{d}x \tag{15}$$

The drag coefficient is monitored during the simulation. Data are collected once the drag coefficient oscillations around the mean value vary by only 1% of the mean value.

1.4 *Solution verification method*

Solution verification is important to estimate the numerical errors and grid uncertainties of a CFD simulation. Numerical errors are due to the numerical solution of the mathematical equations. Aspects of the simulation that cause numerical errors include: discretization, artificial dissipation, incomplete iterative and grid convergence, and computer round-off. To determine numerical errors generally involves performing a sensitivity study by varying the mesh spacing and/or time step size to a smaller value and evaluating the solution differences. Here S_1, S_2, S_3 represent the fine, medium, and coarse grid solutions of any variable in the simulations, respectively. The relative percentage difference ($\delta\%$) between CFD results and correlation values, represented below as A, is calculated as,

$$\delta_{\%} = \left|\frac{A - S_1}{A}\right| \times 100\% \tag{16}$$

The solution verification method in place is the factor of safety method[22,23] which requires the use of the following equations with the use of L2 norm for profiles[24],

$$\varepsilon_{21} = S_2 - S_1 \tag{17}$$

$$\varepsilon_{32} = S_3 - S_2 \tag{18}$$

$$\langle R_G \rangle = \frac{\|\varepsilon_{21}\|_2}{\|\varepsilon_{32}\|_2} \tag{19}$$

$$\langle p_G \rangle = \frac{\ln\left(\frac{\|\varepsilon_{32}\|_2}{\|\varepsilon_{21}\|_2}\right)}{\ln(r_G)} \tag{20}$$

where r_G is the grid refinement ratio, $\Delta x_{G_2} / \Delta x_{G_1}$ and

$\Delta x_{G_3}/\Delta x_{G_2}$, $\varepsilon_{\#\#}$ is the Change between $\hat{S}_{\#}$ for different grids, $S_{\#}$ is the value of a given variable with the grid refinement specified in the subscript. Monotonic convergence is achieved when $0<(R_G)<1$. The ratio of the estimated order of accuracy to the theoretical order of accuracy of the numerical scheme is defined as,

$$P=\frac{\langle p_G\rangle}{p_{th}} \tag{21}$$

where $\langle p_G\rangle$ is the profile averaged order of accuracy, p_{th} is the theoretical order of accuracy, $\langle R_G\rangle$ is the profile averaged convergence ratio.

The closer *P* is to 1 the closer the CFD simulation to the asymptotic range. The estimated error (δ_{RE}) and grid uncertainty (U_G) are defined as,

$$\delta_{RE}=\frac{\varepsilon_{21}}{r^{p_G}-1} \tag{22}$$

$$U_G=[1.6P+2.45(1-P)]\left|\delta_{RE}\right|,\quad 0<P\le 1 \tag{23a}$$

$$U_G=[1.6P+14.8(P-1)]\left|\delta_{RE}\right|,\quad P>1 \tag{23b}$$

where the grid uncertainty, U_G, is presented as a percentage of the correlation value or value from the fine grid solution at the same streamwise location. A lower magnitude of U_G usually indicates a better quality of CFD results.

1.5 *Analysis method*

The viscous dissipation for the mean velocity profile is the only contributor to entropy generation in laminar flow[1]. Therefore, pointwise entropy generation rate equation applied for steady, two-dimensional, laminar boundary layer flows without significant fluctuations is,

$$TS'''\{y\}\approx\mu\left(\frac{\partial U}{\partial y}\right)^2 \tag{24}$$

However, the flow considered herein is unheated. Hence, the entropy generation occurs only due to the square of the gradients of the mean streamwise velocity. The integral over the boundary layer of the pointwise entropy generation rate provides the entropy generation rate per unit area,

$$TS''=\int_0^{\delta}S'''\mathrm{d}y \tag{25}$$

The dissipation coefficient, C_d, is a dimensionless variable that represents the entropy generation rate per unit area. The correlation by McEligot and Walsh estimate the dissipation coefficient multiplied by Re_θ as,

$$C_dRe_\theta=0.1740+0.3315\lambda+0.7881\lambda^2 \tag{26}$$

Both the displacement thickness and momentum thickness are integrated to δ in place of the upper indefinite bound. Fluctuations in bypass transitional flows necessitate additional terms to the entropy generation equations used for laminar flow. These equations are outlined further by Walsh et al.[1].The dimensionless entropy generation rate per unit area for a transitional flow is calculated as,

$$(S''\{\delta\})^+\approx\int_0^{\delta}\left(\frac{\partial U^+}{\partial y^+}\right)^2\mathrm{d}y^+-\int_0^{\delta}(\overline{uv})^+\left[\left(\frac{\partial U^+}{\partial y^+}\right)\right]\mathrm{d}y^+-$$

$$\int_0^{\delta}[\overline{(u'^2)^+}-\overline{(v'^2)^+}]\frac{\partial U^+}{\partial x^+}\mathrm{d}y^+-$$

$$\frac{\mathrm{d}}{\mathrm{d}x^+}\left[\int_0^{\delta}\frac{U^+}{2}\overline{(q^2)^+}\mathrm{d}y^+\right] \tag{27}$$

The variables in Eq.(27), are defined as,

$$(S'')^+=\frac{TS''}{\rho u_\tau^3},\quad (S''')^+=\frac{T\nu S'''}{\rho u_\tau^4},\quad U^+=\frac{U}{u_\tau},\quad u_\tau=\sqrt{\frac{\tau_w}{\rho}},$$

$$x^+=\frac{xu_\tau}{\nu},\quad y^+=\frac{yu_\tau}{\nu},\quad q^2=u'^2+v'^2+w'^2 \tag{28}$$

where u', v', w' are the velocity fluctuations in the x, y and z directions, respectively. The dimensionless form of Eq.(27) is the dissipation coefficient,

$$C_d=(S''\{\delta\})^+\left(\frac{C_f}{2}\right)^{3/2} \tag{29}$$

where C_f, the skin-friction coefficient, is calculated as,

$$C_f=\frac{\tau_w}{\rho U_{fs}^2\{x\}} \tag{30}$$

Intermittency is a measure for determining the laminar, transition, and turbulent regions of the flow and is calculated as,

$$\gamma = \frac{C_f - C_{f,\text{lam}}}{C_{f,\text{turb}} - C_{f,\text{lam}}} \tag{31}$$

where the skin friction coefficient variables for the laminar and turbulent regions are calculated respectively as,

$$C_{f,\text{lam}} = \frac{0.664}{Re_x^{0.5}}, \quad C_{f,\text{turb}} = \frac{0.455}{\ln^2(0.06Re_x)} \tag{32}$$

The intermittency is compared to transition length,

$$\eta_f = \frac{x - x_s}{x_e - x_s} \tag{33}$$

where the x value for the beginning of transition, x_s, is when $\gamma = 0.005$ and the x value for the end of transition, x_g, is when $\gamma = 0.095$.

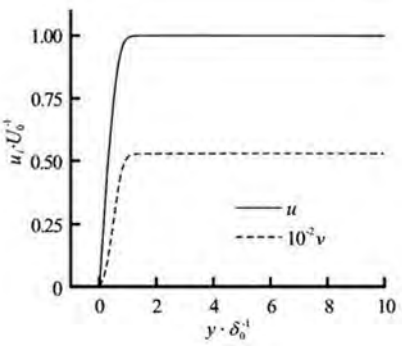

Fig.1 Mean velocity profile at inlet

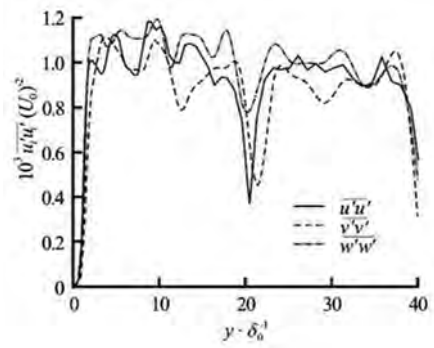

Fig.2 Reynolds normal stress profiles at inlet

2. Simulation design and verification

2.1 *Geometry and flow conditions*

The length of the plate, L_x, is the same as the DNS, i.e., $L_x / \delta_0 = 900$ and 600 for the zero pressure gradient (ZPG) and adverse pressure gradient (APG) cases, respectively. A curved top wall is used to generate the desired pressure gradients within the flow field. The curvature of the top wall is extracted from the DNS grid points and the top wall shape matches the geometry of the DNS[17]. An outflow boundary condition is applied to the domain outlet. A slip wall boundary condition is applied at the top wall whereas a no-slip wall boundary is applied at the plate surface. A velocity inlet boundary conditions is applied to the domain inlet by specifying a mean inlet Blasius velocity profile at $Re_{\delta 0} = U_{fs}\delta_0 / \nu = 800$. The mean profiles of velocities (u, v) and turbulent structure properties (k and ε or ω) are specified as boundary condition at the inlet to the domain and the inlet turbulence is based on the mean Reynolds stresses from the DNS mean statistics. The DNS employs an unsteady inlet using Orr-Somerfiled and squire modes whereas the current study is at steady state. The dimensionless inlet profiles are shown in Fig.1-Fig.3.

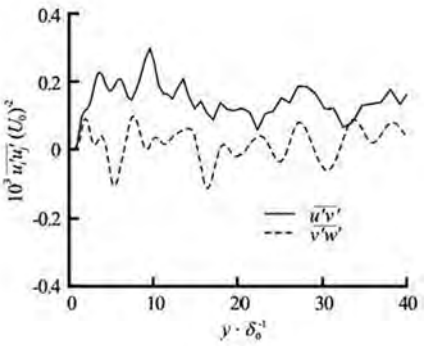

Fig.3 Reynolds shear stress profile at inlet

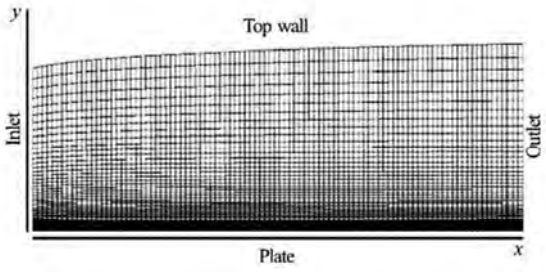

Fig.4 Geometry and mesh representation

The ε and ω values at the inlet and for all models, are estimated using the equations from the ANSYS FLUENT User's Guide[25] as,

$$\varepsilon = \frac{0.09^{3/4}k^{3/2}}{0.4\delta_0}, \quad \omega = \frac{0.09^{-1/4}\sqrt{k}}{0.4\delta_0} \tag{34}$$

While the Reynolds shear stresses are specified directly at the inlet for the RSM. The use of the inlet mean

Table 1 Simulation design table

Flow type	Viscous models	$L_x \times L_y \times L_z$ (m)	$n_x \times n_y \times n_z$	y^+
ZPG	K-ε, SST K-ω, RSM, 4 equation K-ω SST	23.5×1.05×0	3 163×317×0	0.05
($\mathrm{APG}_{\mathrm{weak}}$: $\beta = -0.08$, $\mathrm{APG}_{\mathrm{strong}}$: $\beta = -0.14$)	K-ε, SST K-ω, RSM, 4 equation K-ω SST	15.7×1.05×0	3 163×317×0	0.05

profiles from DNS in the current study is more accurate boundary conditions compared to those applied by Ghasemi et al.[18] wherein the inlet boundary condition is specified with a constant turbulent intensity of 3% and a turbulent length scale equal to the boundary layer thickness.

2.2 *Mesh and simulation table*

The mesh is created in Pointwise v17.0R1. The grid points in the streamwise direction are uniform and the grid points in the plate-normal direction are clustered near the plate surface, as shown in Fig.4. To assign more grid points toward the wall ensures that enough grid points exist within the boundary layer to capture the high velocity gradients in the boundary layer. A medium mesh and a coarse mesh were created for the solution verification study using a constant grid refinement ratio $2^{1/2}$. Figure 4 shows a schematic representation of the domain with an exaggerated curvature of top wall. The figure is a representation of an adverse pressure gradient geometry and mesh. The coordinate axis and boundaries are labeled.

A general overview of the different simulations performed in this study is contained in Table 1.

Table 2 Solution verification for bypass transitional boundary layer flow

	Re_θ	C_f
R_G	0.6640	0.6135
P_G	1.1814	1.4097
P	0.5907	0.7049
$U_G(\%S_1)$	1.5082	0.0020

2.3 *Solution verification*

The results from the solution verification study for the k-ω model are shown in Table 2. The distance to the asymptotic range ($P_G = 1$) is shorter for Re_θ than C_f. Monotonic convergence is achieved. The grid uncertainty is below $1.6\%S_1$ for both variables. The solution verification study shows that the bypass transition results are independent of the grid resolution and thus all results are presented on the fine grid.

3. Results and discussion

The bypass transition simulation results are compared with the DNS results from Nolan and Zaki[17]. Additionaly, the ZPG results are compared to the CFD results by Ghasemi et al.[18] and APG results with Ghasemi et al.[19]. The current simulations employ a more accurate inlet conditions and much finer mesh than the simulations by Ghasemi et al. The k, ω, z, profiles and Reynolds stress values are prescribed at the inlet, depending on the model in use, to match the conditions of the DNS simulation. Ghasemi et al. applied a velocity inlet boundary with a specified turbulent intensity of 3% and a turbulent length scale, whereas the mean velocity and turbulent structure profiles obtained from DNS[17] data are specified at the inlet in the current study. Additionally, this study also examines both CFD predictions for entropy generation rates compared to that post-processed from DNS results.

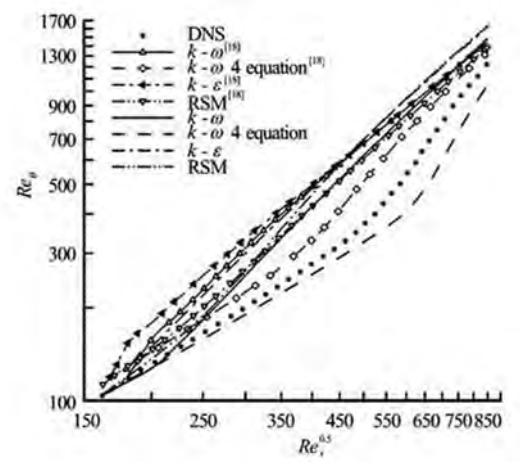

Fig.5 Re_θ versus $Re_x^{1/2}$

3.1 *Zero pressure gradient (ZPG)*

Figure 5 shows how Re_θ varies with $Re_x^{1/2}$. Figure 6 shows a more detailed view near the inlet region. The DNS data is linear in the log-log scale, the slope remains small up to $Re_x^{1/2} = 450$ and then the slope becomes much steeper indicating the onset of transition from laminar to turbulent boundary layer profile. The k-ε model follows the DNS results near the inlet until $Re_x^{1/2} = 180$ where it transitions to tur-

bulence. However, in that range results from Gashemi et al.[18] show a steep slope and transition right at the inlet and much further away from DNS results. The RSM model shows similar trend like the $k-\varepsilon$ model but the results from Gashemi et al. are further away from the DNS.

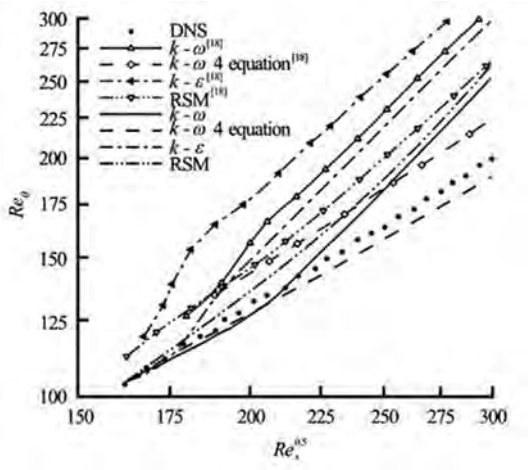

Fig.6 Re_θ versus $Re_x^{1/2}$ (detailed view near inlet)

The $k-\omega$ model shows very close agreement to the DNS until $Re_x^{1/2}=215$ and then deviates downstream whereas Gashemi et al. shows transition much earlier at $Re_x^{1/2}=185$ and has a much larger difference in magnitude of Re_θ. The $k-\omega$ 4 equation model results closely resemble the DNS results compared to all other simulations but the magnitude remains slightly lower than DNS data throughout the domain and the change in slope occurs at $Re_x^{1/2}=575$ later than $Re_x^{1/2}=475$ from DNS. The $k-\omega$ 4 equation model for Gashemi et al. shows transition much earlier than DNS at $Re_x^{1/2}=325$. The results in this study agree much better with the DNS results than the results from Ghasemi et al.[18] in terms of overall magnitude of predicted Re_θ and the location of transition for all corresponding models.

Figure 7 and Fig.8 show how C_f and C_d vary with $Re_x^{1/2}$, respectively. The dissipation coefficient, C_d, provides a measure of the pointwise entropy generation rate, S''' (in non-dimensional form), within the boundary layer for ZPG case as described earlier. The DNS data has a linear slope in the turbulent regime. The laminar region is the initial downward slope, the rise indicates the transition region, and the small oscillations downstream are within the fully turbulent region. Figure 7 also shows the analytical laminar and turbulent lines. Similar to the trends seen in Fig.5, the $k-\varepsilon$ model and RSM transition to turbulent profile very close to the inlet and remain turbulent throughout the flow field.

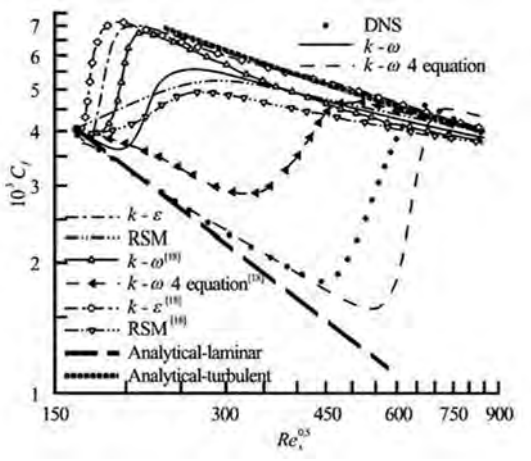

Fig.7 C_f versus $Re_x^{1/2}$

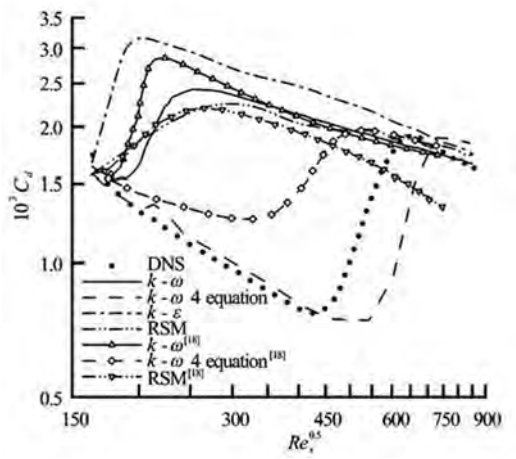

Fig.8 C_d versus $Re_x^{1/2}$

In Fig.7, the $k-\varepsilon$ model shows an initial laminar profile near the inlet, similar to DNS, before transition occurs downstream. The $k-\omega$ model shows a laminar region until $Re_x^{1/2}=215$, where the onset of transition is predicted by the model. The $k-\omega$ model shows close agreement of predicted C_f to the DNS data from the inlet until the onset of transition and also in the turbulent region but transition occurs upstream compared to the $k-\omega$ 4 equation model and the DNS data. The $k-\omega$ 4 equation model shows better agreement with the DNS data for both C_d and C_f. The C_d and C_f predicted by the $k-\omega$ 4 equation model is very accurate compared to the DNS data until the transitional point in DNS at $Re_x^{1/2}=450$. The model, however, over predicts the location of the onset of transition which occurs much later than DNS at $Re_x^{1/2}=575$.

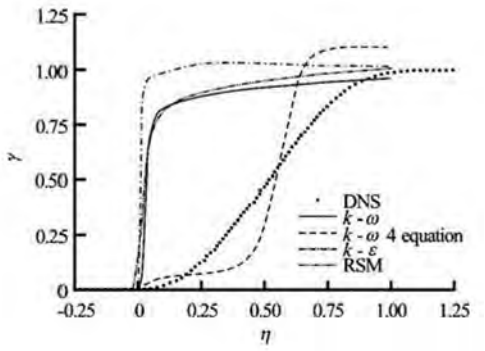

Fig.9 γ versus η

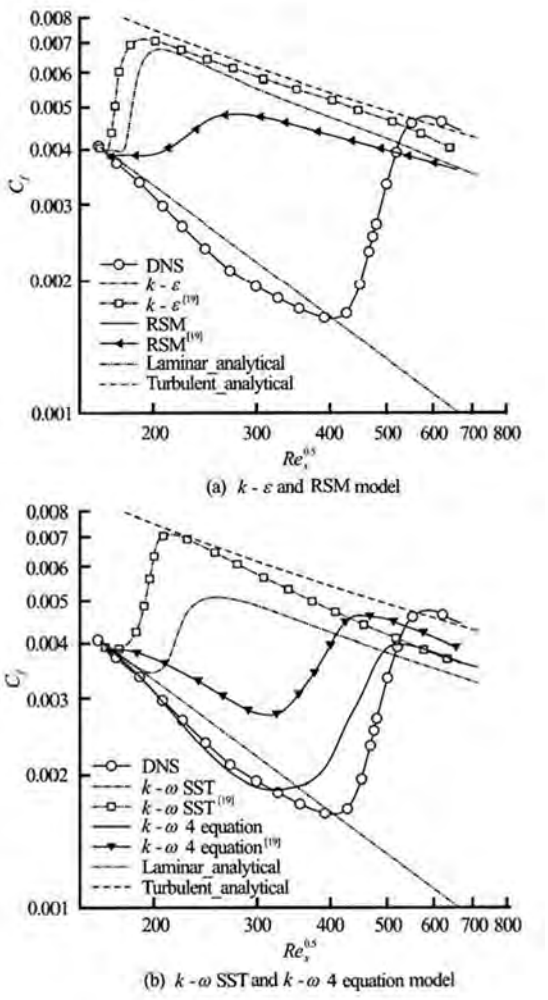

Fig.10 C_f versus $Re_x^{1/2}$ for various RANS models for $\mathrm{APG}_{\mathrm{weak}}$

Figure 9 shows that all turbulence models examined in this study predict transition onset ($\gamma \le 0.05$) earlier than the DNS data. The k-ω, k-ε, and RSM's demonstrate very similar trends with steeper slopes than the k-ω 4 equation models. The k-ω 4 equation model is the closest to the DNS data in predicting the transition onset location but over-predicts γ by as much as 10% in the fully turbulent region. All models tend to predict a much steeper slope in the transition region compared to the much smoother slope in the DNS data.

3.2 *Adverse pressure gradient (APG)*

The bypass transition simulation results for APG cases are also compared to the DNS results from Nolan and Zaki[17] and the CFD results by Ghasemi et al.[19]. The APG results are evaluated using the skin-friction coefficient, C_f, and the approximate pointwise entropy generation rate, S'''.

3.2.1 $\mathrm{APG}_{\mathrm{weak}}$: $\beta = -0.08$

Figure 10 shows comparison of C_f predicted from various models along the length of the flat plate versus $Re_x^{1/2}$ on a log-log scale for the weak APG case. The C_f from DNS deviates from the analytical Blasius laminar approximation at about $Re_x^{1/2} = 200$ and is lower in the laminar region than the analytical approximation. The DNS predicts the onset of transition at about $Re_x^{1/2} = 400$ and fully developed turbulent flow beyond $Re_x^{1/2} = 550$. Figure 10(a) and Figure 10(b) show the k-ε, RSM, k-ω SST and transitional k-ω 4 equation models compared with results from DNS and Ghasemi et al.[19] for the same models. The k-ε, RSM, k-ω SST and k-ω 4 equation models predict onset of transition at $Re_x^{1/2}$ = 170, 200, 220 and 350, respectively. All the above models compare better with DNS in predicting transition occurrence further downstream than by the corresponding models from Ghasemi et al.. The transition k-ω 4 equation model predicts the flow very accurately and follows the DNS prediction very closely throughout the domain especially in the laminar and transition regimes. All four models in the present study under predict the skin-friction coefficient magnitude in the fully turbulent regime. Overall the results from this study are comparatively more accurate and in line with the DNS results than the results from Ghasemi et al.[19] in terms of trends and magnitude for all corresponding models especially, the transitional k-ω 4 equation model.

The under prediction of C_f in the fully turbulent regime compared to Ghasemi et al.[19] is due to the differences in the inlet boundary conditions specified. Specifying a constant turbulent intensity of 3% and a specific length scale rather a mean profile for turbulent structures as in the simulations by Ghasemi et al. could result in over prediction of fully turbulent regime compared to the actual capabilities of each RANS model.

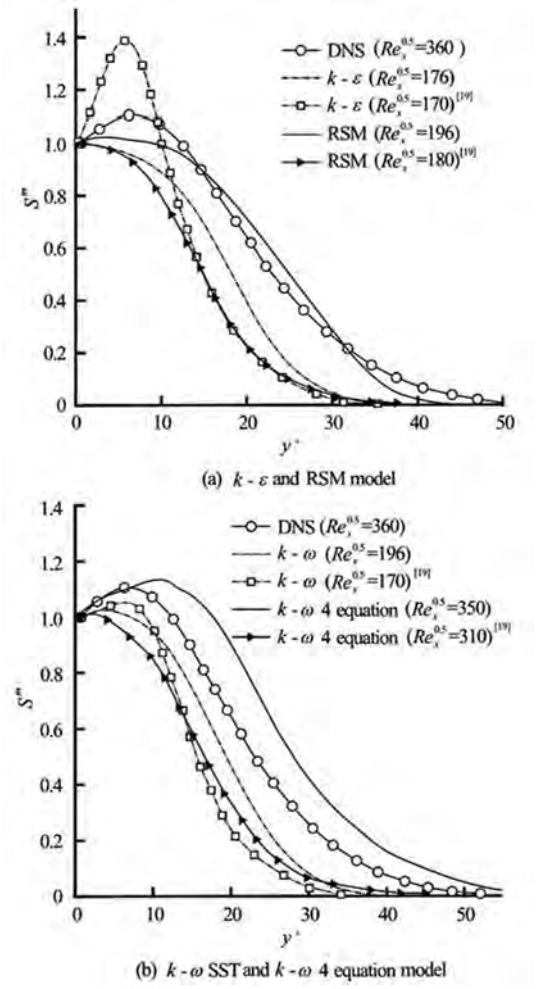

Fig.11 S''' versus y^+ for various RANS models for $\mathrm{APG}_{\mathrm{weak}}$ near location of transition shown by values of $Re_x^{1/2}$

Figure 11 shows the comparison of approximate point-wise entropy generation rates, S''', as predicted by each model within the boundary layer plotted normal to the wall in terms of y^+. Since different models predict varying locations of transition, the entropy generation rate (S''') comparison is made at different locations along the flat plate for each model. These locations (indicated by $Re_x^{1/2}$ values) are selected at a point near the onset of transition as predicted by each model.

Figure 11(a) shows the k-ε and RSM model and Figure 11(b) shows the k-ω SST and transitional k-ω 4 equation models compared with results from DNS and Ghasemi. As seen from the figures the predictions from the current study are more accurate in terms of trends, magnitude and location than from Ghasemi for all corresponding models compared to DNS values. This is a direct result of better resolution within the boundary layer using more grid points near the wall and keeping $y^+ < 1$ at the first grid point away from the plate. The predictions from the k-ε, RSM and k-ω SST are considerably closer to DNS values than Ghasemi et al.. The transitional k-ω 4 equation model is the most accurate among all models although it slightly over-predicts the magnitude of S'''.

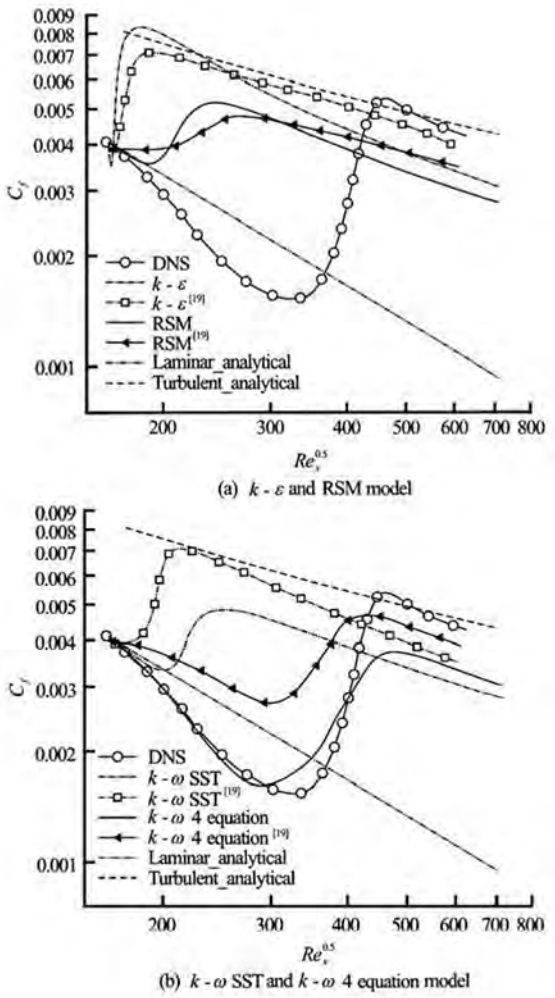

Fig.12 C_f versus $Re_x^{1/2}$ for various RANS models $\mathrm{APG}_{\mathrm{Strong}}$

3.2.2 $\mathrm{APG}_{\mathrm{strong}}$: $\beta = -0.14$

Figure 12 shows the comparison of C_f predicted from various models along the length of the flat plate versus $Re_x^{1/2}$ on a log-log scale. The DNS[17] results show that C_f deviates from the Blasius laminar approximation at approximately $Re_x^{1/2} = 180$ and predicts a lower C_f value in the laminar region as seen in the previous $\mathrm{APG}_{\mathrm{weak}}$ case.

The stronger adverse pressure gradient causes an earlier shift on predicted C_f from the analytical app-

roximation. The DNS predicts the onset of transition at about $Re_x^{1/2} = 330$ and fully developed turbulent flow beyond $Re_x^{1/2} = 450$. The Stronger APG also shows an increase the maximum magnitude of S''' from 1.1 in the $\mathrm{APG}_{\mathrm{weak}}$ case to a value of 1.5.

Figure 12(a) show the $k-\varepsilon$ and RSM model and Fig.12(b) shows the $k-\omega$ SST and transitional $k-\omega$ 4 eqation models. The $k-\varepsilon$, RSM, $k-\omega$ SST and $k-\omega$ 4 equation models predict onset of transition at $Re_x^{1/2}$ = 170, 195, 210 and 290, respectively. The $k-\varepsilon$ model transitions to fully turbulent flow near the inlet for the current study as in the study by Ghasemi et al.. This may be a result of the stronger pressure gradient being imposed on the flow and thereby indicating the models incapability in handling strong adverse pressure gradients effectively. The RSM, $k-\omega$ SST and $k-\omega$ 4 equation models follow similar trends as seen in the $\mathrm{APG}_{\mathrm{weak}}$ case with better comparison to DNS values than that by Ghasemi et al.[19].

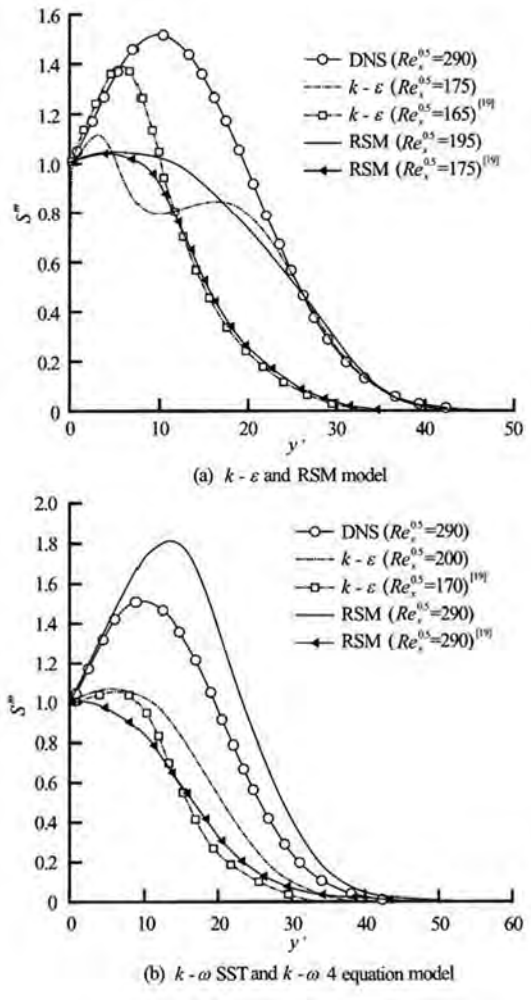

Fig.13 S''' versus y^+ for various RANS models $\mathrm{APG}_{\mathrm{Strong}}$

Following the trend seen in previous results the models in current study under predict magnitude of C_f in the fully turbulent regime. Possible causes for such under prediction maybe as noted earlier in $\mathrm{APG}_{\mathrm{Weak}}$ results.

Figure 13 shows the comparisons of predicted approximate point-wise entropy generation rate S''' within the boundary layer normal to the wall near the location of transition point in terms of y^+. It is noteworthy that, since the $k-\varepsilon$ model transitions near the inlet under the strong adverse pressure gradient, Fig.13(a) shows a turbulent profile of predicted entropy generation rate at $Re_x^{1/2} = 175$ for this model. The RSM, $k-\omega$ SST and $k-\omega$ 4 equation models predict more accurate comparable profiles for S''' near their transition location than the models by Ghasemi et al..

4. Conclusions and future work

This study evaluates the capability of various RANS models to predict entropy generation rates in bypass transitional boundary layer flows with and without pressure gradients. The results show significant improvements over the RANS results by Ghasemi et al.[18,19] for all comparable models due to the employment of a much finer grid and more accurate inlet boundary conditions for velocity and turbulent structures.

Overall, the results from this study are more accurate and comparable to the DNS results than the results from Ghasemi for both $\mathrm{APG}_{\mathrm{weak}}$ and $\mathrm{APG}_{\mathrm{strong}}$ cases with respect to trends and magnitude for all corresponding RANS models except for slight under prediction of magnitude within the fully turbulent regime. Better grid resolution within the boundary layer also helps predict the approximate pointwise entropy generation rate profiles for adverse pressure gradient cases more closely to DNS than Ghasemi et al.[19]. $\mathrm{APG}_{\mathrm{strong}}$ has a higher maximum value of S''' in the boundary layer than $\mathrm{APG}_{\mathrm{weak}}$ case indicating a direct relationship between the pressure gradient and entropy generation rates. The results suggest that the $k-\omega$ 4 equation model accurately predicts the boundary layer behavior and entropy generation for bypass transitional flows. All other models predict transition onset upstream of the location shown by the DNS data. However, the $k-\omega$ transition 4 equation model slightly over predicts the onset of transition from the DNS data based on the skin friction coefficient for the ZPG case and under predicts in the APG cases.

In the future, the capability of using different

LES models to predict entropy generation rates for bypass transitional flows with and without streamwise pressure gradients will be evaluated. Sensitivity of LES models to grid resolution and time step size will be examined following the recent general framework for LES verification and validation[26,27]. The use of unsteady hydrodynamic instabilities in velocity and turbulent structure profiles at the inlet may lead to more accurate CFD predictions for bypass transitional boundary layer flows for both RANS and LES models.

Acknowledgements

This work was supported by the U.S. Department of Energy, Office of Science, Basic Energy Sciences, under Award # DE-SC0004751. The authors would also like to thank Dr. Tamer Zaki, Dr. Kevin Nolan, and Dr. Edmond Walsh for meaningful contributions.

References

[1] WALSH E. J., MCELIGOT D. M. and BRANDT L. et al. Entropy generation in a boundary layer transitioning under the influence of freestream turbulence[J]. **Journal of Fluids Engineering,** 2011, 133(6): 061203.

[2] ZAKI T. A., DURBIN P. A. Mode interaction and the bypass route to transition[J]. **Journal of Fluid Mechanics,** 2005, 531(1): 85-111.

[3] MCELIGOT D. M., WALSH E. J. and LAURIEN E. et al. Entropy generation in the viscous parts of turbulent boundary layers[J]. **Journal of Fluids Engineering,** 2008, 130(6): 061205.

[4] SPALART P. R. Direct simulation of a turbulent boundary layer up to $Re_\theta = 1410$ [J]. **Journal of Fluid Mechanics,** 1988, 187(1): 61-98.

[5] SPALART P. R. Numerical study of sink-flow boundary layers[J]. **Journal of Fluid Mechanics,** 1986, 172(1): 307-328.

[6] ROTTA J. Turbulent boundary layers in incompressible flow[J]. **Progress in Aerospace Sciences,** 1962, 2(1): 1-95.

[7] MCELIGOT D. M., WALSH E. J. and LAURIEN E. et al. Entropy generation in the viscous layer of a turbulent channel flow[R]. Idaho National Laboratory (INL), 2006.

[8] ABE H., KAWAMURA H. and MATSUO Y. Direct numerical simulation of a fully developed turbulent channel flow with respect to the reynolds number dependence[J]. **Journal of Fluids Engineering,** 2001, 123(2): 382-393.

[9] KRAUSE E., OERTEL H. J. and SCHLICHTING H. **Boundary-layer theory**[M]. New York, USA: Springer, 2004.

[10] MCELIGOT D. M., NOLAN K. P. and WALSH E. J. Effects of pressure gradients on entropy generation in the viscous layers of turbulent wall flows[J]. **International Journal of Heat and Mass Transfer,** 2008, 51(5-6): 1104-1114.

[11] TSUKAHARA T., SEKI Y. and KAWAMURA H. et al. DNS of turbulent channel flow at very low Reynolds numbers[C]. **Proceedings of the 4th International Symposium on Turbulence and Shear Flow Phenomena.** Williamsburg, USA, 2005, 935-940.

[12] WALSH E. J., MCELIGOT D. M. A New correlation for entropy generation in low Reynolds number turbulent shear layers[J]. **International Journal of Fluid Mechanics Research,** 2009, 36(6): 566-572.

[13] ABE H., KAWAMURA H. and MATSUO Y. Surface heat-flux fluctuations in a turbulent channel flow up to $Re_\tau = 1020$ with $Pr = 0.025$ and 0.71[J]. **International Journal of Heat and Fluid Flow,** 2004, 25(3): 404-419.

[14] HOYAS S., JIMÉNEZ J. Scaling of the velocity fluctuations in turbulent channels up to $Re = 2003$ [J]. **Physics of fluids,** 2006, 18(1): 011702.

[15] SCHLATTER P., BRANDT L. and De LANGE H. et al. On streak breakdown in bypass transition[J]. **Physics of fluids,** 2008, 20(1): 101505.

[16] BRANDT L., SCHLATTER P. and HENNINGSON D. S. Transition in boundary layers subject to free-stream turbulence[J]. **Journal of Fluid Mechanics,** 2004, 517: 167-198.

[17] NOLAN K., ZAKI T. A. Conditional sampling of transitional boundary layers in pressure gradients[J]. **Journal of Fluid Mechanics,** 2013, 728: 306-339.

[18] GHASEMI E., MCELIGOT D. and NOLAN K. et al. Entropy generation in a transitional boundary layer region under the influence of freestream turbulence using transitional RANS models and DNS[J]. **International Communications in Heat and Mass Transfer,** 2012, 41(1): 10-16.

[19] GHASEMI E., MCELIGOT D. M. and NOLAN K P. et al. Effects of adverse and favorable pressure gradients on entropy generation in a transitional boundary layer region under the influence of freestream turbulence[J]. **International Journal of Heat and Mass Transfer,** 2014, 77(1): 475-488.

[20] ANSYS. "FLUENT theory guide v14.0.0."[R]. 2011.

[21] XING T., BHUSHAN S. and STERN F. Vortical and turbulent structures for KVLCC2 at drift angle 0, 12, and 30 degrees[J]. **Ocean Engineering,** 2012, 55(3): 23-43.

[22] XING T., STERN F. Closure to "Discussion of "Factors of safety for Richardson extrapolation"' (2011, Journal of Fluids Engineering, 133, 115501)[J]. **Journal of Fluids Engineering,** 2011, 133(11): 115502.

[23] XING T., STERN F. Factors of safety for richardson extrapolation[J]. **Journal of Fluids Engineering,** 2010, 132(6): 061403.

[24] WILSON R. V., STERN F. and COLEMAN H. W. et al. Comprehensive approach to verification and validation of CFD simulations–Part 2: Application for rans simulation of a cargo/container ship[J]. **Journal of Fluids Engineering,** 2001, 123(4): 803-810.

[25] ANSYS. "FLUENT user guide v14.0.0."[R]. 2011.

[26] XING T., GEORGE J. Quantitative verification and validation of large eddy simulations[C]. **ASME 2014 Verification and Validation Symposium.** Las Vegas, Nevada, USA, 2014.

[27] XING Tao. A general framework for verification and validation of large eddy simulations (keynote speaker)[C]. **Proceedings of the 13th National Congress on Hydrodynamics and 26th Conference on Hydrodynamics.** Qingdao, China, 2014, 40-58.